https://doi.org/10.5194/egusphere-2026-6481
Preprint. Discussion started: 5 November 2026
© Author(s) 2026. CC BY 4.0 License.

Joint Contribution of Spatiotemporal Factors and Chemical Composition on the Hygroscopicity of Aerosol Particles in the Southern Great Plains

Kyle McCary[1] , Rylen Pereira[1] , Alan Gonzalez[2] , Xiangxinyue Meng[1] , Ajith Thenoor Chandran[1], Heewon Yim[2] , Maria A. Zawadowicz[3] , John E. Shilling[4] , Qi Ying[2] , Yue Zhang[1, *]

[1]*Department of Atmospheric Sciences, Texas A&M University, College Station, TX, 77843, USA*
[2]*Zachry Department of Civil and Environmental Engineering, Texas A&M University, College Station, TX, 77843, USA*
[3]*Department of Environmental Science and Technologies,* Brookhaven *National Laboratory, Upton, NY, 11973, USA*
[4]*Pacific Northwest National Laboratory, Richland, WA, 99354, USA*

Correspondence to: Yue Zhang (yuezhang@tamu.edu)

Abstract. Aerosol source and composition strongly affect the ability of particles to act as cloud condensation nuclei (CCN), influencing precipitation and radiative forcing. This study employs aircraft data from the Holistic Interactions of Shallow Clouds, Aerosols, and Land-Ecosystems (HI-SCALE) campaign over the Southern Great Plains to quantify activated fraction and CCN closure under varying environmental conditions. Hybrid Positive Matrix Factorization was implemented for source apportionment across spring and fall for air masses originating from four U.S. regions. An external mixture best represented the aerosol, and organic hygroscopicity depended strongly on air mass origin and altitude, increasing above 2000 m. Multivariable linear regression showed that organic hygroscopicity correlates not only with chemical composition but also with air mass origin, temperature, and relative humidity, underscoring the need to consider both air mass and chemistry when modeling aerosol-cloud interactions.

1 Introduction

Aerosols have a significant influence on the formation of clouds in the atmosphere by acting as cloud condensation nuclei (CCN) (Fan et al., 2016; Duplissy et al., 2008; Hobbs, 1993). Such aerosol-cloud interactions carry long-term climatological implications through radiative forcing (Mülmenstädt and Feingold, 2018; Anwar et al., 2022; Rosenfeld et al., 2014). Through the Twomey and Albrecht effects, aerosols indirectly influence Earth's radiation budget by modifying cloud microphysical and radiative properties (Twomey, 1977; Albrecht, 1989; Rissman et al., 2004). CCN can also contribute to short-term mesoscale meteorology differences through suppressing drizzle and affecting local precipitation rates (Albrecht, 1989; Anwar et al., 2022). Understanding the underlying physical and chemical properties of aerosol species, especially their

https://doi.org/10.5194/egusphere-2026-6481
Preprint. Discussion started: 5 November 2026
© Author(s) 2026. CC BY 4.0 License.

CCN properties that result in the formation of clouds, is essential for current and future modeling of aerosol-cloud interactions (Anwar et al., 2022; Duplissy et al., 2008; Fan et al., 2016; Mülmenstädt and Feingold, 2018; Rosenfeld et al., 2014; Andreae, 1995; Intergovernmental Panel on Climate, 2023). Specifically, a key parameter in determining the activity of CCN in the environment is hygroscopicity, a size-independent parameter which relates to the ability of a particle to uptake water (Petters and Kreidenweis, 2007). One approach in determining this hygroscopicity parameter for ambient datasets is by interpreting chemical and Cloud Condensation Nuclei Counter (CCNC) data together in a closure analysis (Kulkarni et al., 2023; Meng et al., 2014; Bhattu and Tripathi, 2015).

Previous studies conducted CCN closures through field measurements, providing important information regarding the aerosol properties and their subsequent CCN activity for region-scale modeling (Ren et al., 2018; Bhattu and Tripathi, 2015; Broekhuizen et al., 2006; Miao et al., 2015; Kulkarni et al., 2023; Vanreken et al., 2003; Srivastava et al., 2013; Meng et al., 2014). Several field studies employed ground-based data to perform these closure analyses (Ren et al., 2018; Bhattu and Tripathi, 2015; Broekhuizen et al., 2006; Miao et al., 2015; Meng et al., 2014; Jayachandran et al., 2017; T. C. et al., 2022). For instance, Meng et al. 2014 analyzed a month of ground-based measurements in Hong Kong in a closure analysis to determine the sensitivity of CCN counts to mixing state and supersaturation. Despite the breadth of CCN closure analyses described above, previous research often focused on surface-based measurements (Srivastava et al., 2013; Vanreken et al., 2003; Ren et al., 2018; Broekhuizen et al., 2006; Meng et al., 2014). In addition, different regions of the United States have had locally dependent CCN closure studies completed (Vanreken et al., 2003), however cross-comparisons between regions' aerosol physical and chemical properties are limited. There have been limited laboratory studies and targeted ground-based field measurements that examine the relationship between specific dominant organic aerosol species and their hygroscopicity (Duplissy et al., 2011; Massoli et al., 2010; Chang et al., 2010; Kuang et al., 2020). Aircraft field campaigns have also been implemented to conduct closure analyses, although the amount of aircraft data is limited compared to surface-based data (Vanreken et al., 2003; Kulkarni et al., 2023; Srivastava et al., 2013; Park et al., 2020). Access to data with vertical profiles, would allow for insight into the cloud-relevant altitudes at which the physicochemical properties of aerosols most strongly influence CCN formation.

The HI-SCALE campaign spanned across multiple seasons with different altitudes, providing a rich dataset that allows for comprehensive analysis to bridge the above knowledge gap of few studies above the surface (Fast et al., 2019; Fast et al., 2016; Shilling, 2023; Wang, 2016). This field study took place in the central United States, specifically near the Southern Great Plains (SGP), where the air mass origin, altitude, and seasonality could drastically alter aerosol composition and hygroscopicity (Loveland et al., 1995). Such changes allow for detailed analysis regarding the impacts of spatiotemporal factors on CCN properties due to differences in the physical and chemical properties of aerosols (Falah et al., 2022). Combining multi-season, regional, and altitude data into one CCN closure study allows for comprehensive coverage of the determining factors in CCN activity. Kulkarni et al. 2023 analyzed a single day of the HI-SCALE dataset, determining the mixing state of aerosol species that results in the most consistent estimation of organic hygroscopicity (Kulkarni et al., 2023). However, the seasonality and the associated chemical dependence of hygroscopicity remains largely uncertain (Kulkarni et al., 2023).

https://doi.org/10.5194/egusphere-2026-6481
Preprint. Discussion started: 5 November 2026
© Author(s) 2026. CC BY 4.0 License.

Airborne field measurements such as the HI-SCALE campaign allows for organic hygroscopicity interpretation in a novel method, as the dataset provides both the altitude and regionality necessary for a more robust prediction of the bulk organic hygroscopicity at a scale unlike other studies and can provide pivotal information to modelers in region-based organic hygroscopicity implementation in cloud modeling (Dinar et al., 2008; Ovadnevaite et al., 2011).

In this study, a CCN hygroscopicity closure analysis and PMF were performed on the 2016 HI-SCALE campaign aircraft dataset spanning two seasons, to examine the impacts of mixing state, air mass origin, seasonality, and chemical composition on organic hygroscopicity. The PMF results were then integrated into a multivariable linear regression model to determine the impacts of chemical, physical, and environmental properties on organic hygroscopicity. Discussions of the discrepancies between analysis methodologies for CCN closures, as well as oxygen to carbon (O:C) and hydrogen to carbon (H:C) ratio analysis in comparison to modeling of region-specific organic hygroscopicity provide further understanding of the CCN activity in the SGP region.

2 Materials and Methods

2.1 HI-SCALE Data

The data for this study came from the 2016 HI-SCALE campaign taking place around the SGP Atmospheric Radiation Measurement (ARM) site in northern Oklahoma, and the data employed in this study ranged from April 25th to September 17th, with April and May representing the Spring and August and September representing the Fall (Fast et al., 2016; Shilling, 2023; Wang, 2016). The flights ranged in length from 67 minutes to 352 minutes after data cleaning, such as removal of zeroes and outlier points, has been implemented, with the flight list in Table S1. A representation of one of these flights is shown in Figure S1, alongside the location of the SGP site. The flights ran in legs, where the aircraft would fly at specific altitudes for a consistent amount of time. Data that was marked as suspect either by an instrument flag or by the instrument PI was removed from the study. The instruments in this campaign were a Cloud Condensation Nuclei Counter (CCNC; Droplet Measurement Technologies, Longmont, CO, USA), a Condensation Particle Counter (CPC; TSI Incorporated, Shoreview, MN, USA), a High-Resolution Time-of-Flight Aerosol Mass Spectrometer (HR-ToF-AMS; Aerodyne Research Inc., Billerica, MA, USA) for non-refractory chemical composition, a Fast Integrated Mobility Spectrometer (FIMS) for aerosol size distributions, and GPS data for location and altitude (Decarlo et al., 2006; Jayne et al., 2000; Lance et al., 2006; Roberts and Nenes, 2005; Wang et al., 2017). Due to the close overlap between the measurement size range of the FIMS, ranging from 10 nm to 600 nm, and the HR-ToF-AMS, with a peak transmission efficiency of ~50 nm to 500 nm, we assumed the size distribution measured by FIMS were representative of the AMS chemical species data, as there is no other size-dependent chemical composition data available (Wang et al., 2018; Liu et al., 2007). Correction for differences between the diameters and confirmation for the diameter ranges capturing the correct ranges for this study is shown in SI Section 1 and Figure S2. The CCNC was run at two set supersaturations during the entirety of the campaign, specifically 0.24% and 0.46%. All of the available data was resampled

https://doi.org/10.5194/egusphere-2026-6481
Preprint. Discussion started: 5 November 2026
© Author(s) 2026. CC BY 4.0 License.

to a one-minute time resolution, which allowed for the alignment of all-time series for data analysis. The campaign-long time series of all of the available data is shown in Figure S3.

2.2 Air Mass Origin Determination

In order to determine the origin of air masses at specific altitudes, 72-hour HYSPLIT back trajectory analyses at the targeted altitude and location were employed (Draxler and Rolph, 2010). Splitting back trajectories into four different regions allowed for large and robust datasets for each region. These regions are designated as the West, the Midwest, the Southeast, and the Gulf, defined by their distinctive climatology, topography, and geography (Arguez et al., 2012). Figure 1 displays the regions listed above. The West region represents that the air mass originated from either the southwest or northwest, and west of the Rocky Mountains, containing an arid and dry climate. The Midwest region is defined as air masses from the north and the northeast (or the Great Lakes region), all east of the Rocky Mountains, controlled by temperate climates and Great Lake influences. The Southeast region includes air masses that originate east of the SGP site and south of 37 degrees N latitude, defined by densely wooded areas and a subtropical climate. The Gulf region is defined as air masses whose origin lies in the Gulf of Mexico and is defined separately from the Southeast to attempt to display differences between land origin and ocean origin air masses.

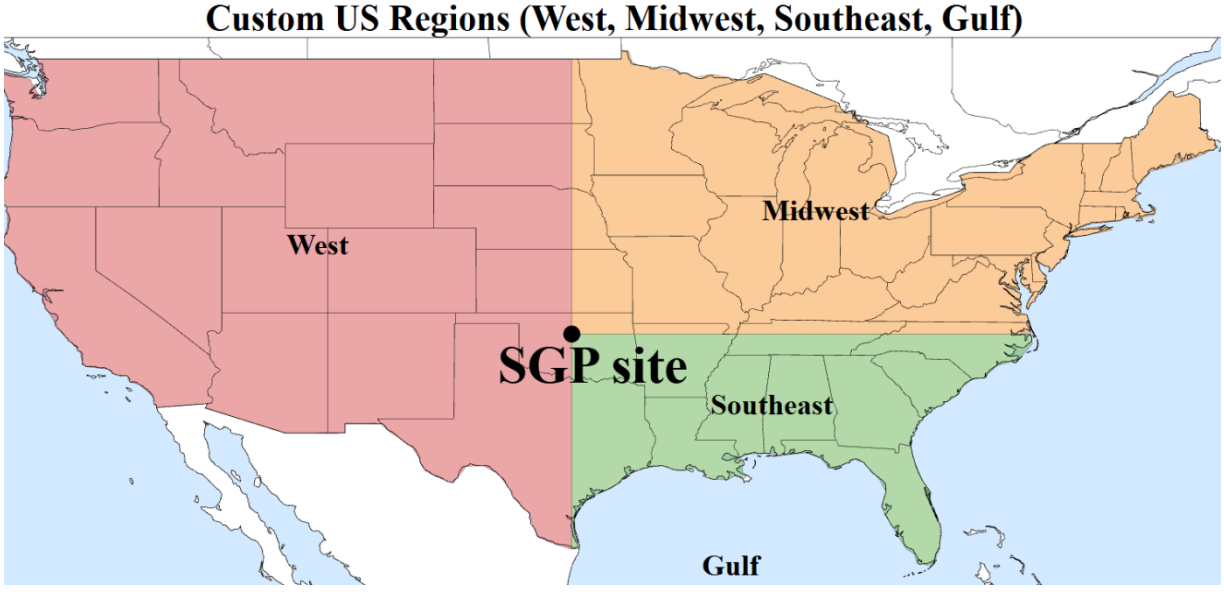


Figure 1. A map displaying the regions of interest in relation to the SGP measurement site.

https://doi.org/10.5194/egusphere-2026-6481
Preprint. Discussion started: 5 November 2026
© Author(s) 2026. CC BY 4.0 License.

2.3 Data Analysis Methodology

2.3.1 Organic Hygroscopicity vs. Closure Ratio Curves

In the process of running the closure analysis, a closure ratio was determined through the modeled activated fraction divided by the measured activated fraction of particles. Our organic hygroscopicity was calculated by varying the input organic hygroscopicity until reaching a closure ratio of 1, similar to other studies (Kulkarni et al., 2023). Using the HR-ToF-AMS data, mass concentrations were converted into moles so that ion assignment can be performed (Gysel et al., 2007). This may introduce error by assuming an organic molar mass, but a straight mass to volume conversion does not allow for sulfate ion assignment. The breakdown of the fraction of sulfate broken into ammonium sulfate, ammonium bisulfate, and sulfuric acid is shown in Figure S4 (Gysel et al., 2007). Subsequently, molar concentrations were converted into volumes using molar mass and density. Therefore, the volume fraction (ε) for each ion can be calculated by Equation (Eq.) 1.

$$\varepsilon_i = volume_i / volume_{total} \quad (1)$$

Similar to other studies in the same region, 20% of organic aerosols were assumed to be insoluble (Kulkarni et al., 2023). The activated fraction was calculated by dividing the measured CCN counts by the measured CPC counts. Internally mixed aerosols were assumed to be the bulk composition, meaning each particle is made up of all species present divided by mass percentage, measured by the HR-ToF-AMS, while externally mixed particles were assumed to consist of a single species: organic, sulfate, nitrate, and any other species contained within the HR-ToF-AMS data (Li et al., 2016; Kulkarni et al., 2023). For this closure study, organic hygroscopicity was varied from 0.02 to 0.50 as an input parameter during the data analysis to determine the optimum organic hygroscopicity. A calculation of total hygroscopicity for the bulk aerosol is achieved with Eq. 2 for the internally mixed assumption (Petters and Kreidenweis, 2007).

$$\kappa_{int} = \sum_i \varepsilon_i \kappa_i \quad (2)$$

The critical diameter (D_{crit}) was calculated with Eq. 3 from κ-Köhler theory, implementing the hygroscopicity from Eq. 2, where D_d represents the critical diameter and S_c represents the saturation ratio (1.0024 and 1.0046, respectively for our calculations) (Petters and Kreidenweis, 2007). In Eq. 3 and 4, $\sigma_{s/a}$ is the surface tension of water at 0.072 J/m^2, T is temperature at 298.15 K, with R being the gas constant and M_w and ρ_w being the molecular weight and density of water (Petters and Kreidenweis, 2007).

$$\kappa = \frac{4A^3}{27 D_d^3 \ln^2(S_c)} \quad (3)$$

$$A = \frac{4\sigma_{s/a} M_w}{RT\rho_w} \quad (4)$$

The calculated critical diameter, D_{crit}, is then applied to the FIMS distribution to determine the activated fraction of particles for the chemical-based calculation. If D_{crit} values lie in between a bin, the estimated number of particles is interpolated in order to produce a curve instead of assuming a whole bin is activated.

For the external mixing assumption, the D_{crit} of each species is calculated with Eq. 3 using literature values for hygroscopicity, written in Table S2 (Petters and Kreidenweis, 2007; Seinfeld and Pandis, 2016). Each of these D_{crit} for all

https://doi.org/10.5194/egusphere-2026-6481
Preprint. Discussion started: 5 November 2026
© Author(s) 2026. CC BY 4.0 License.

chemical species is then compared to the FIMS data to produce an activated fraction for individual species. To derive an externally mixed estimated activated fraction, activated fractions are weighted by volume fractions with Eq. 5.

$$AF_{ext} = \sum_i AF_i * \varepsilon_i \quad (5)$$

The method for calculating the closure ratio is the same for both mixing states after the model activated fractions are calculated. Closure ratio values for each organic hygroscopicity values are derived from dividing the modeled activated fractions by the actual measured activated fractions. The mean closure ratios for each region are calculated, and plotted against organic hygroscopicity, as shown in Figure 2. The closure ratio equal to 1 is defined as the modeled organic hygroscopicity value matches with the measured activated fraction.

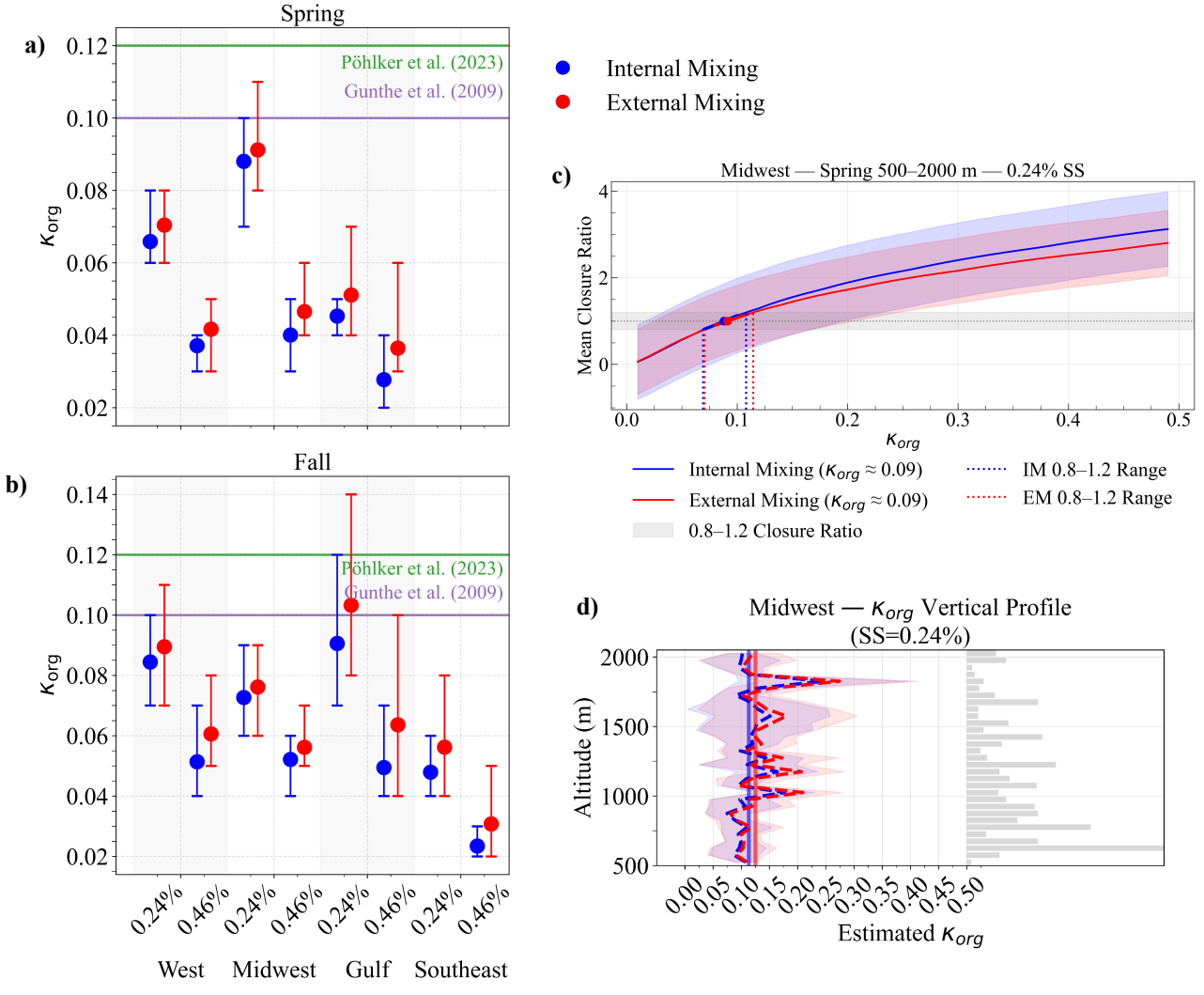


Figure 2. The estimated organic hygroscopicity values for each region, based on the methodology Section 2.3.1. Figure 2a is Spring, and Figure 2b is Fall, with literature values for comparison (Pöhlker et al., 2023; Gunthe et al., 2009). There is no Spring data for the Southeast. The error bars are the 0.8 to 1.2 range of organic hygroscopicity values, as seen in Figure 2c and Figures S5-S9. There

https://doi.org/10.5194/egusphere-2026-6481
Preprint. Discussion started: 5 November 2026
© Author(s) 2026. CC BY 4.0 License.

were no statistically significant changes between seasons for any region, with statistical methods described in SI Section 4. In Figure 2d is an example of the vertical estimation methodology in Section 2.3.2.

2.3.2 Vertical Organic Hygroscopicity Profiles

Vertical profiles of modeled organic hygroscopicity for each region were also calculated. The closure ratio of the vertical profile was calculated differently compared with Section 2.3.1 and led to different results. The best fit organic hygroscopicity was derived on a point-by-point basis, instead of taking the mean for each region then determining where the closure ratio curve crosses 1. As the previous section is a bulk calculation, encompassing the whole flight, this methodology is required to obtain a point-by-point measurement. The individual points are then summed into vertical bins of 50 m. The order of operations difference affects modeled organic hygroscopicity, and the deviations will be discussed in Section 3.3. A comparison of this methodology and the Section 2.3.1 methodology is shown in the flowchart in Figure 3.

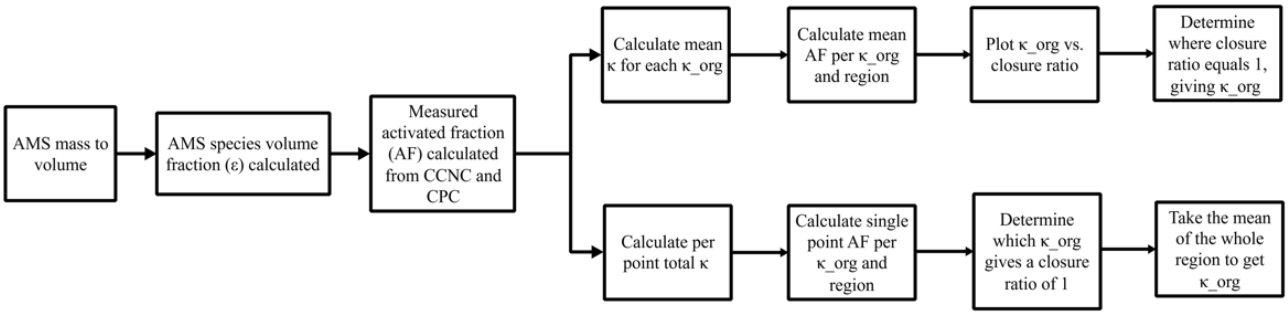


Figure 3. Methodology for the closure analysis, defining the split between the bulk methodology and the vertical single-point methodology.

2.3.3 PMF Analysis Methodology

Multivariable PMF analysis was performed on the HR-ToF-AMS mass spectra data with the ME-2 Engine (Drosatou et al., 2019; Brown et al., 2015; Nursanto et al., 2023; Ajith et al., 2024). The goal of PMF analysis is to determine if specific factors are region specific, or if certain organic aerosols are more prevalent during specific season. Further details on the procedure for the PMF analysis are included in SI Section 3. Based on $Q/Q_{expected}$, explained in Section S3.4, the number of factors was determined to be 4. Assignment of these factors is determined from specific fractional organic species contributions to solution spectra compared to other literature (Mohr et al., 2012). The results from multiple ME-2 and PMF Evaluation Tool (PET) solutions were cross compared in order to produce a robust set of factors present in all solutions (Drosatou et al., 2019; Brown et al., 2015).

2.3.4 Multivariable Linear Regression

To further develop the implications of the PMF results, a multilinear regression employing relevant factors to determine their influence on organic hygroscopicity was established on a region-by-region basis (Uyanık and Güler, 2013).

https://doi.org/10.5194/egusphere-2026-6481
Preprint. Discussion started: 5 November 2026
© Author(s) 2026. CC BY 4.0 License.

The equation implemented for this analysis is displayed in Eq. 6, where β represents the coefficient tied to the specific input, ϵ represents the error term, and y represents organic hygroscopicity in this case.

$$y = \beta_0 + \beta_1 * x_1 + \beta_2 * x_2 + \ldots + \beta_n * x_n + \epsilon \quad (6)$$

For our model, input implementation was done in a stepwise fashion to measure the organic hygroscopicity response to increasing model complexity. The simplest model included only organic mass, and complexity increased as organic mass was split into POA and SOA, and then eventually the four PMF factors. Other environmental and physicochemical property-based inputs aside from the total organic mass were geometric mean diameter (GMD), O:C and H:C ratio, ambient temperature, and relative humidity. Table 1 displays the specific inputs for each run of the model in detail. Due to differences in scale between input factors, β coefficients, which define the relationship between a factor and the solution, were standardized such that their impact on organic hygroscopicity can accurately be assessed (Nimon and Oswald, 2013). R^2 of the model determined the portion of the variability in the output y is determined by the inputs x (Nimon and Oswald, 2013). The contribution of each input, explained through standardized β coefficients, are the essential outputs to determine model input efficacy in determining organic hygroscopicity as well as defining factors that affect region-specific organic hygroscopicity (Nimon and Oswald, 2013).

Table 1. The different multivariable linear regression model inputs, based on specific model run and the number of inputs.

Model Factor Number	Model Inputs
1	Org. Mass
2	Org. Mass, GMD
3	POA Mass, SOA Mass, GMD
5	Four ME-2 Factors' Mass, GMD
6	Four ME-2 Factors' Mass, GMD, Ambient Temp.
7	Four ME-2 Factors' Mass, GMD, Ambient Temp. and RH
9	Four ME-2 Factors' Mass, GMD, Ambient Temp. and RH, O:C and H:C Ratios

3 Results and Discussion

3.1 Regional and Seasonal Variability in Bulk Hygroscopicity Closure Analysis

The closure ratio curves for each region are displayed in Figures S5-S9, with the closure ratio plotted on the y-axis and the organic hygroscopicity input value along the x-axis, with both internal and external mixing assumptions presented in different colors. Given there is no noticeable difference in modeled organic hygroscopicity from 500 - 2000 m coupled with minimal variation in chemical composition and aerosol size distributions, the differing factors in this analysis are mainly attributed to season and region. This lack of difference will be discussed in Section 3.3. The modeled organic hygroscopicity

https://doi.org/10.5194/egusphere-2026-6481
Preprint. Discussion started: 5 November 2026
© Author(s) 2026. CC BY 4.0 License.

decreases by 40-50% as the supersaturation increases from 0.24% to 0.46% for all regions, and the external mixing assumption yields slightly higher values for all runs, regardless of region or supersaturation. All hygroscopicity values for this methodology and a representation of one of the closure curves is summarized in Figures 2a-b, with literature comparisons (Gunthe et al., 2009; Pöhlker et al., 2023).

The derived organic hygroscopicity values across all regions were lower than literature values, displaying a slight underprediction for this data set (Pöhlker et al., 2023; Petters and Kreidenweis, 2007; Rickards et al., 2013; Gunthe et al., 2009). Kulkarni et al. 2023 reported that the internal and external mixing assumptions produced modeled organic hygroscopicity values under 0.10, consistent with the results presented in this study. Seasonally, organics in the Fall tend to have 10-20% higher modeled hygroscopicity values than in the Spring. The lowest modeled organic hygroscopicity is in the Southeast region, and the highest is in the Gulf region. The West and Midwest are nearly equivalent in the Fall but differ in other seasons. The shift in hygroscopicity values between the two supersaturations displays the inconsistency that arises with assuming chemical species are equally distributed across a size-spectrum. The mixing state of aerosols is more complex than just internally or externally mixed and without size-resolved chemical data, interpretation of the specific mixing state is difficult (Riemer et al., 2019).

3.2 Altitude-Driven Variability in Organic Hygroscopicity: Regional Insights

The 0.24% results for the vertical binning methodology in Section 2.3.2 for the analysis of the modeled organic hygroscopicity are shown in Figure 2d and Figure S10. As shown, there is no noticeable shift in modeled organic hygroscopicity from 500 - 2000 m for any region, oscillating between roughly ±0.05 of the mean with no definite trend. Figures 2a-b and S10 also show slightly higher values of hygroscopicity as the calculation is based on the mean of the vertical profile. Seasonality was not distinguished in the vertical distribution, but the mean modeled hygroscopicity values still show higher values. Compared to the results in Section 3.1, the 0.24% SS values are in much closer alignment with the generally estimated values of organic hygroscopicity (Petters and Kreidenweis, 2007; Pöhlker et al., 2023; Rickards et al., 2013). The unique data in this vertical distribution analysis is related to the West region, similar to the previous section due to the aircraft traveling above 2000 m. The West curve shifts to the right as altitude increases past 2000 m shown in Figure S10, signifying a noticeable increase in organic hygroscopicity related to the altitude increase. This signals the potential for more oxidized organic species at higher altitudes due to the increase in hygroscopicity values (Han et al., 2022; Cerully et al., 2015; Kuang et al., 2020). High-altitude measurements are only available in two flights, limiting the scope of data interpretation above 2000 m. More studies implementing high altitude (>2000 m) data would provide further insight into the noticeable difference in this dataset (Fast et al., 2016; Shilling, 2023; Wang, 2016).

3.3 Bias in Mean Hygroscopicity Arising from Bulk vs. Vertical Averaging

The discrepancy in mean hygroscopicity values between the Section 3.1 bulk results and Section 3.2 vertical integration results demonstrate an inherent bias when calculating hygroscopicity and warrants further examination. Here, the

https://doi.org/10.5194/egusphere-2026-6481
Preprint. Discussion started: 5 November 2026
© Author(s) 2026. CC BY 4.0 License.

organic hygroscopicity vs. closure ratio curve can be defined as a function f(D_{crit}), represented in Eq. 7. When $f(D_{crit})$ has a non-linear response to D_{crit}, as occurs in Eq. 7 derived from κ-Köhler theory, the point at which the mean is taken carries significance (Petters and Kreidenweis, 2007).

$$\kappa \propto (D_{crit})^{-3} \quad (7)$$

As the organic hygroscopicity value increases, D_{crit} decreases in a non-linear fashion. In this relationship, $f(\text{mean}(D_{crit})) \neq \text{mean}(f(D_{crit}))$, which is known as Jensen's inequality (Bibi and Ali, 2025; Xiao and Lu, 2020). The bulk results in Section 3.1 are represented by $f(\text{mean}(D_{crit}))$, while the vertically determined results from Section 3.2 are represented by $\text{mean}(f(D_{crit}))$. Jensen's inequality dictates for convex functions, $\text{mean}[f(D_{crit})] \geq f(\text{mean}[D_{crit}])$, and vice versa for concave functions (Xiao and Lu, 2020; Bibi and Ali, 2025). If the second derivative of the function is greater than 0 for all D_{crit}, the function is convex (Pratt, 1981). The second derivative of Eq. 7 becomes $12D_{crit}^{-5}$, and given that D_{crit} is always positive, the function is convex for all values of D_{crit}. Hence, the vertical distribution results from Section 3.2 are larger than the mean estimate values from Section 3.1, agreeing with Jensen's inequality and further solidifying the validity of the results from the previous sections. This bias between Section 3.1 and 3.2 hygroscopicity results raises a question about the methods implemented for CCN closure studies. Slight differences in hygroscopicity values could further propagate into other work where hygroscopicity is a defining parameter (Hu et al., 2010). The methodology in Section 3.2 resulted in organic hygroscopicity values that compared more closely to literature values, shown in Figure 2a (Pöhlker et al., 2023; Petters and Kreidenweis, 2007; Rickards et al., 2013; Gunthe et al., 2009). Future studies implementing both methodologies and highlighting the biases from the results would increase understanding of how mathematical methods affect closure results.

3.4 Consistent Four-Factor PMF Solution from Hybrid Size–Composition Analysis

A series of hybrid PMF solutions with both size and chemical composition data were run to determine the best number of factors to explain source apportionment. The ME-2 Engine solution was determined to be the consistent result that had four separate, discernable factors that appeared in all other multi-factor solutions tested. Compared to previous literature, Factors 1-4 from Figure 4 are each determined to be Sulfate-based Semi-volatile Oxidized Organic Aerosol (SB SV-OOA), Nitrate-based Semi-volatile Oxidized Organic Aerosol (NB SV-OOA), Low Volatility Oxidized Organic Aerosol (LV-OOA), and Primary Organic Aerosol (POA), respectively (Mohr et al., 2012). Determination of the SV-OOA factors is from the relationship between *f43* and *f44*, and the inorganic species dominance, and LV-OOA was dominated by the *f44* signal, with a very low *f43* signal. (Mohr et al., 2012). POA is dominated by *f43* as well, but based on HR-fit data, this *f43* signal is roughly 2/3 dominated by hydrocarbons, and all subsequent highest fraction masses of *m/z* 27, 41, 42, 55, 69, and 71 are fully hydrocarbon dominated. Based on the size distributions for each factor, there is general agreement on expectation of increased size with increased oxidation state, as lower volatility factors generally have larger size distributions (Kroll et al., 2015; Nursanto et al., 2023). However, the appearance of smaller sizes in the NB SV-OOA signifies the inclusion of POA in this factor, which is confirmed by a noticeable *f57* signal confirmed to be the hydrocarbon C_4H_9 based on HR-fit data (Mohr et

https://doi.org/10.5194/egusphere-2026-6481
Preprint. Discussion started: 5 November 2026
© Author(s) 2026. CC BY 4.0 License.

al., 2012). The time series of all of the PMF factors are presented in Figure 5. Additional analysis of the PMF results can be found in SI Section 3.

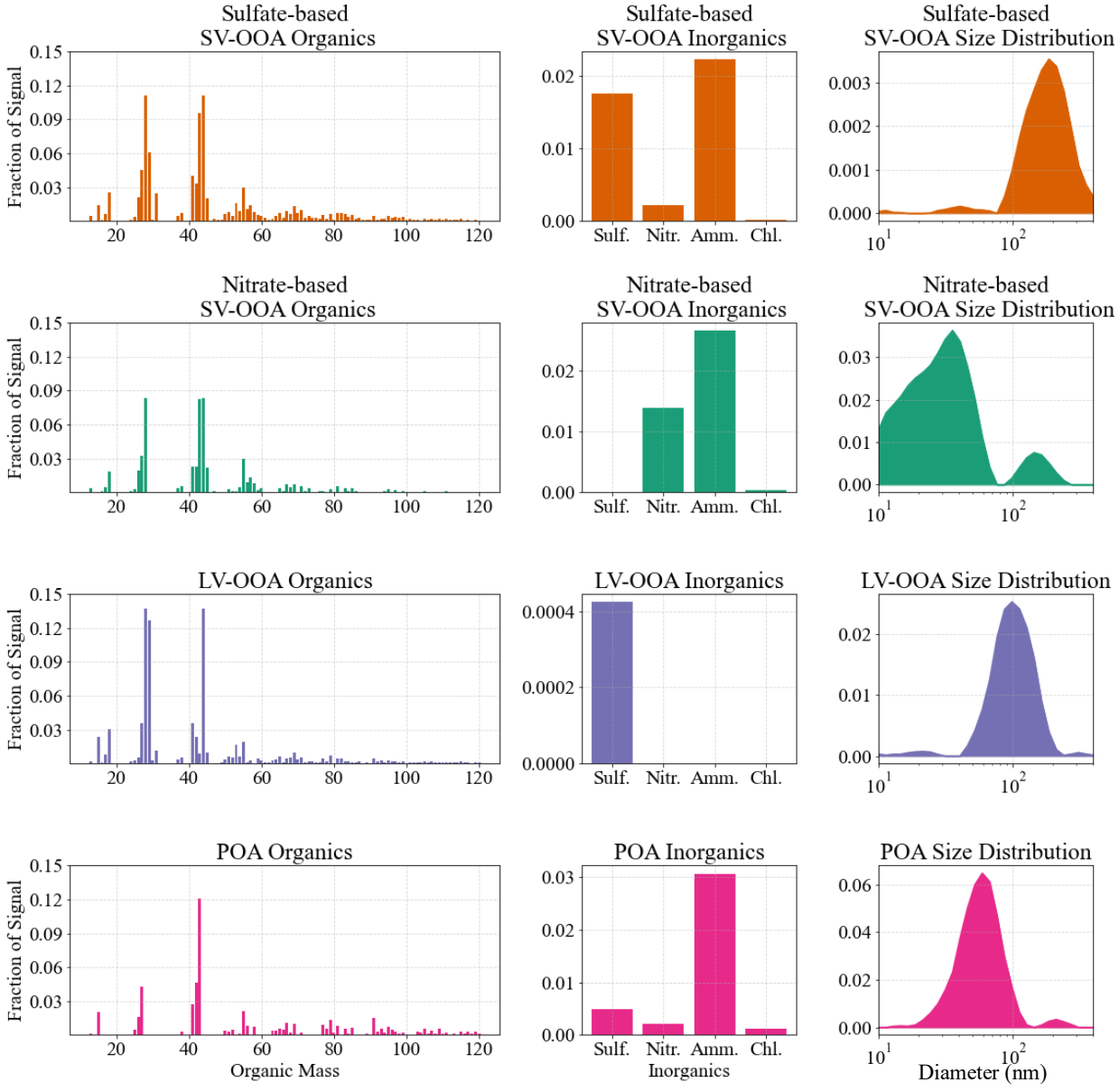


Figure 4. PMF Factors determined through multivariable PMF analysis, with the mass loadings of each of these factors being implemented into the linear regression model.

https://doi.org/10.5194/egusphere-2026-6481
Preprint. Discussion started: 5 November 2026
© Author(s) 2026. CC BY 4.0 License.

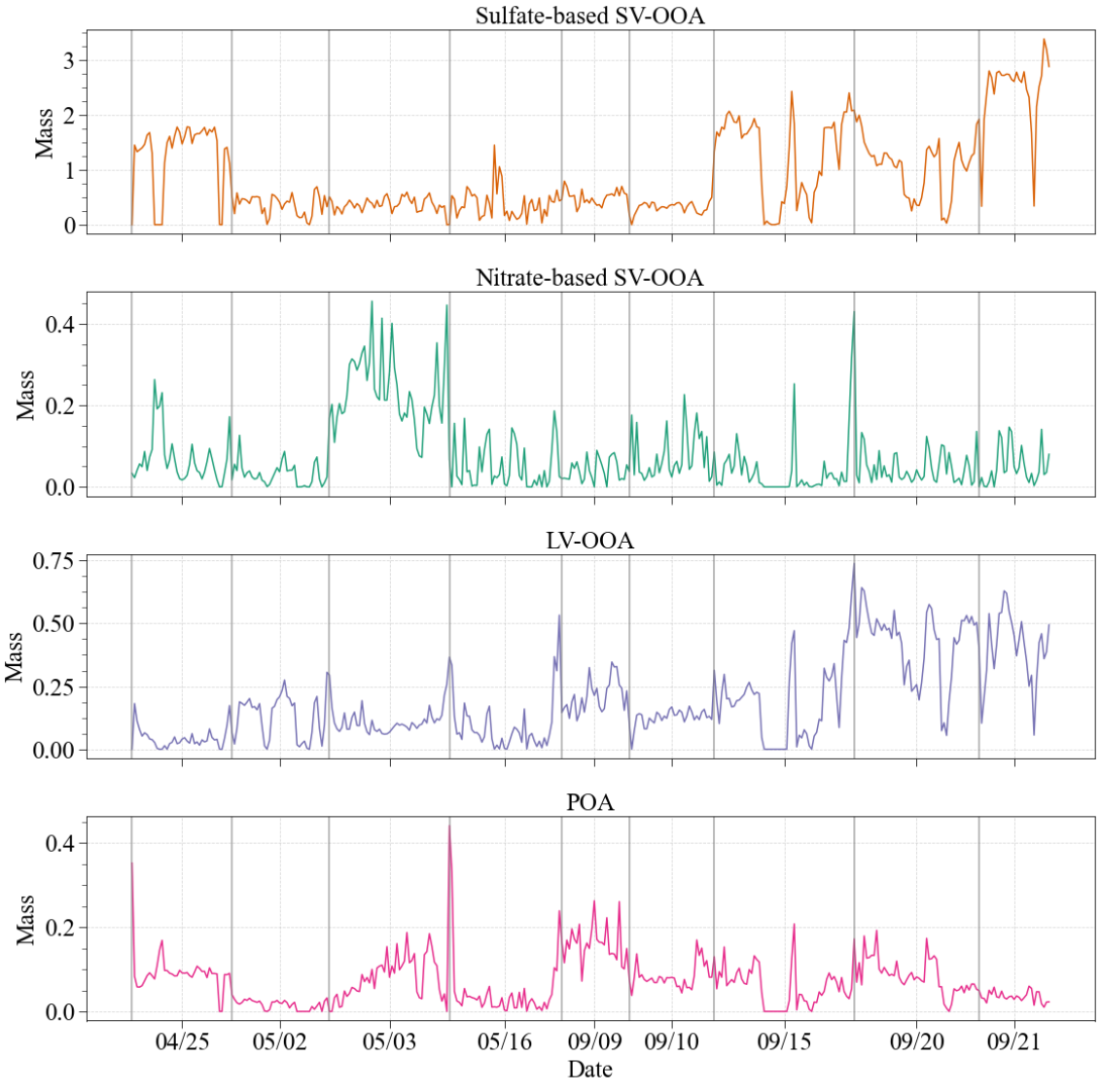


Figure 5. The time series for all the factors from the ME-2 PMF analysis, broken down by date and region origin in μg/m^3.

3.5 Region-Dependent Predictors of Organic Hygroscopicity from Multivariable Regression

275 Previous studies have employed simple chemical composition (oxygen-to-carbon ratio, O:C) to model the organic hygroscopicity. Figure 6a displays the results of the finalized 9-factor multilinear regression with airborne data compared to a model based on O:C ratio only in Figure 6b (Lambe et al., 2011), which does not provide strong correlation. The nine factors, associated with distinct physical and chemical properties, are as follows: Geometric Mean Diameter (GMD), the four PMF factors from Section 3.4, O:C ratio, H:C ratio, and ambient temperature and relative humidity. The factors involved in the

https://doi.org/10.5194/egusphere-2026-6481
Preprint. Discussion started: 5 November 2026
© Author(s) 2026. CC BY 4.0 License.

formula for each region are in Table 2. For the Gulf and the Midwest regions, over 70% of the variability in organic hygroscopicity can be explained by the input factors. The contribution of all inputs is 20 to 30% less in the Southeast and West regions, indicating higher complexity in determining correlative factors with organic hygroscopicity. O:C ratio carries the strongest impact on total R^2 for the Gulf Region, indicating for this dataset that Gulf-originated organics' hygroscopicity is heavily influenced by oxidation state. The most impactful factor is LV-OOA mass loadings in the Midwest, indicating oxidation state also plays a role, but the concentration of these LV-OOA species and their microphysical properties also contributes. In both the Southeast and West regions, from our data, size carries the largest significance in organic hygroscopicity. Each region's model output contains unique information about how each region's organic species is affected by different intrinsic and extrinsic properties as shown in Figures 7-8.

Figure 6 displays the introduction of a higher number of parameters into modeling organic hygroscopicity produces a substantial improvement in organic hygroscopicity for each data point. The inclusion of PMF factors alleviates the lack of strong positive correlation between solely O:C ratio and organic hygroscopicity, with the detailed parameterization of hygroscopicity in Table 2.

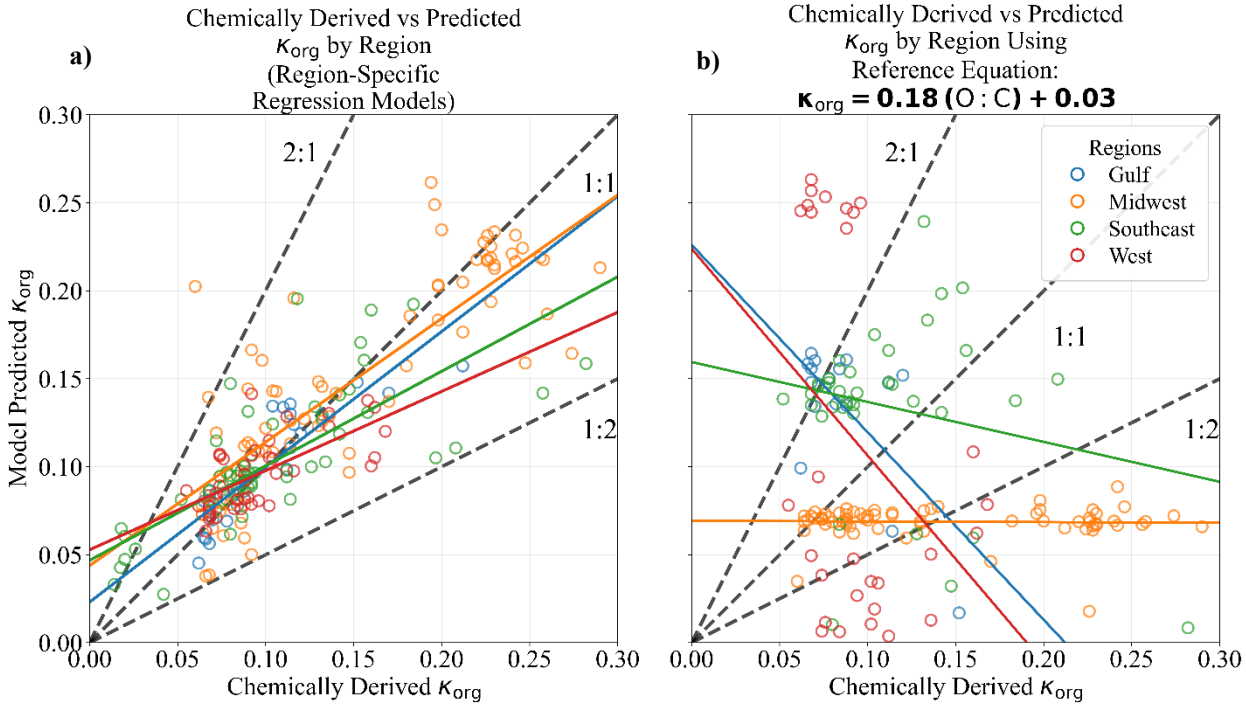


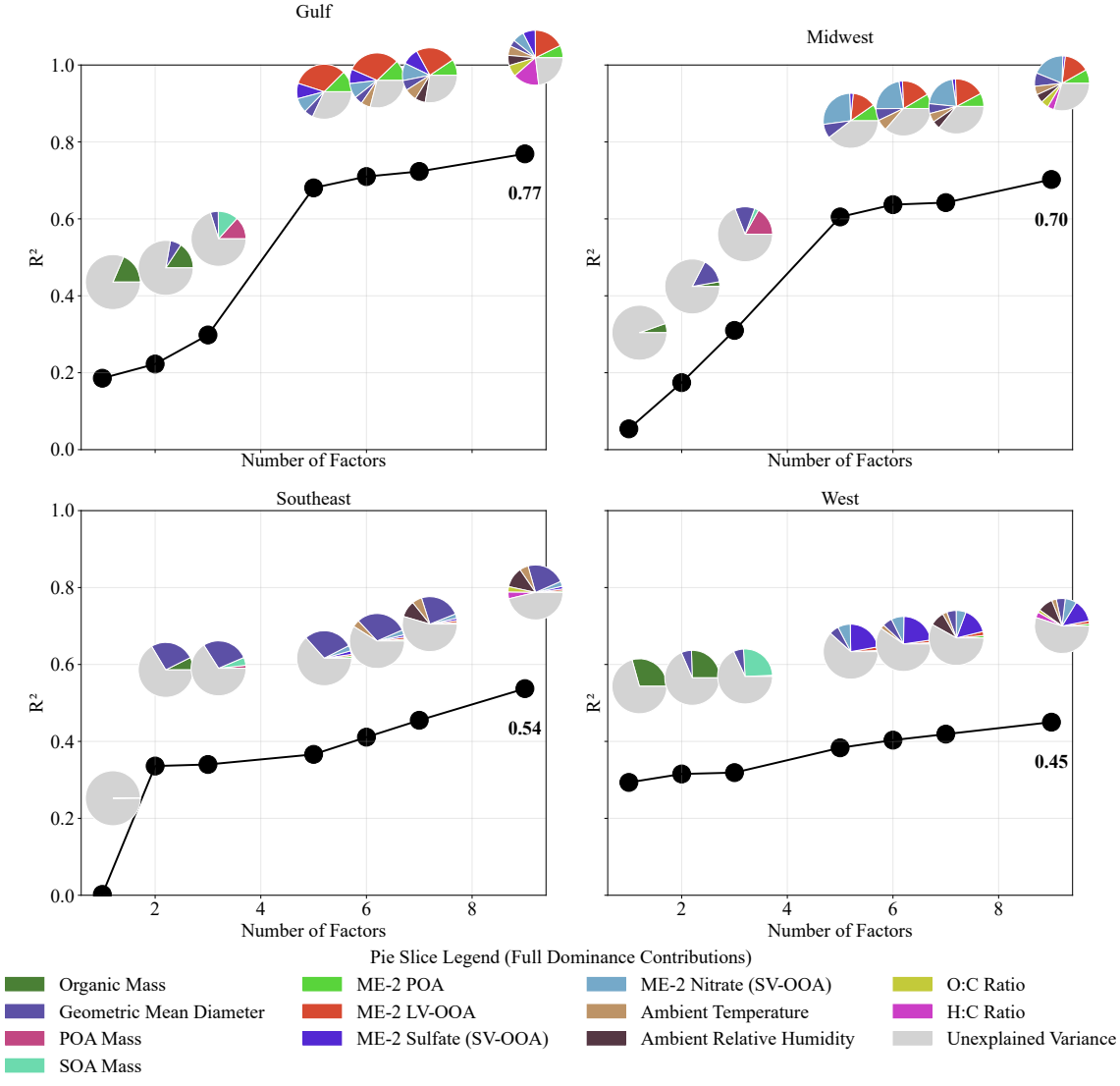
Figure 6. The relationship between model-derived and chemically derived hygroscopicity values, with the Figure 6a displaying our finalized 9-factor model and Figure 6b displaying a literature model relating solely to O:C ratio (Lambe et al., 2011).

https://doi.org/10.5194/egusphere-2026-6481
Preprint. Discussion started: 5 November 2026
© Author(s) 2026. CC BY 4.0 License.

Table 2. The coefficients for each factor of the 9-factor model, and the inputs used for the calculation in Figure 6.

Parameter	Gulf	MW	SE	W
POA	0.189	-0.088	-0.144	0.278
LV-OOA	0.239	0.446	-0.012	0.323
Sulfate SV-OOA	-0.000	-0.091	0.407	-0.458
Nitrate SV-OOA	-0.272	-0.400	-0.292	0.355
Geometric Mean Diameter	-0.068	0.286	-0.590	0.481
Ambient Temp.	-0.012	-0.355	-0.492	-0.603
Ambient RH	0.354	-0.170	-0.500	-0.423
O:C Ratio	0.648	0.934	0.424	0.416
H:C Ratio	0.905	0.576	0.736	0.494
R^2	0.77	0.70	0.54	0.45

https://doi.org/10.5194/egusphere-2026-6481
Preprint. Discussion started: 5 November 2026
© Author(s) 2026. CC BY 4.0 License.



300

Figure 7. The iterations of the model, with pie charts above each iteration displaying model parameter contribution to the variance of κ_{org}. The factors implemented at each number of factors are displayed in Table 1.

https://doi.org/10.5194/egusphere-2026-6481
Preprint. Discussion started: 5 November 2026
© Author(s) 2026. CC BY 4.0 License.

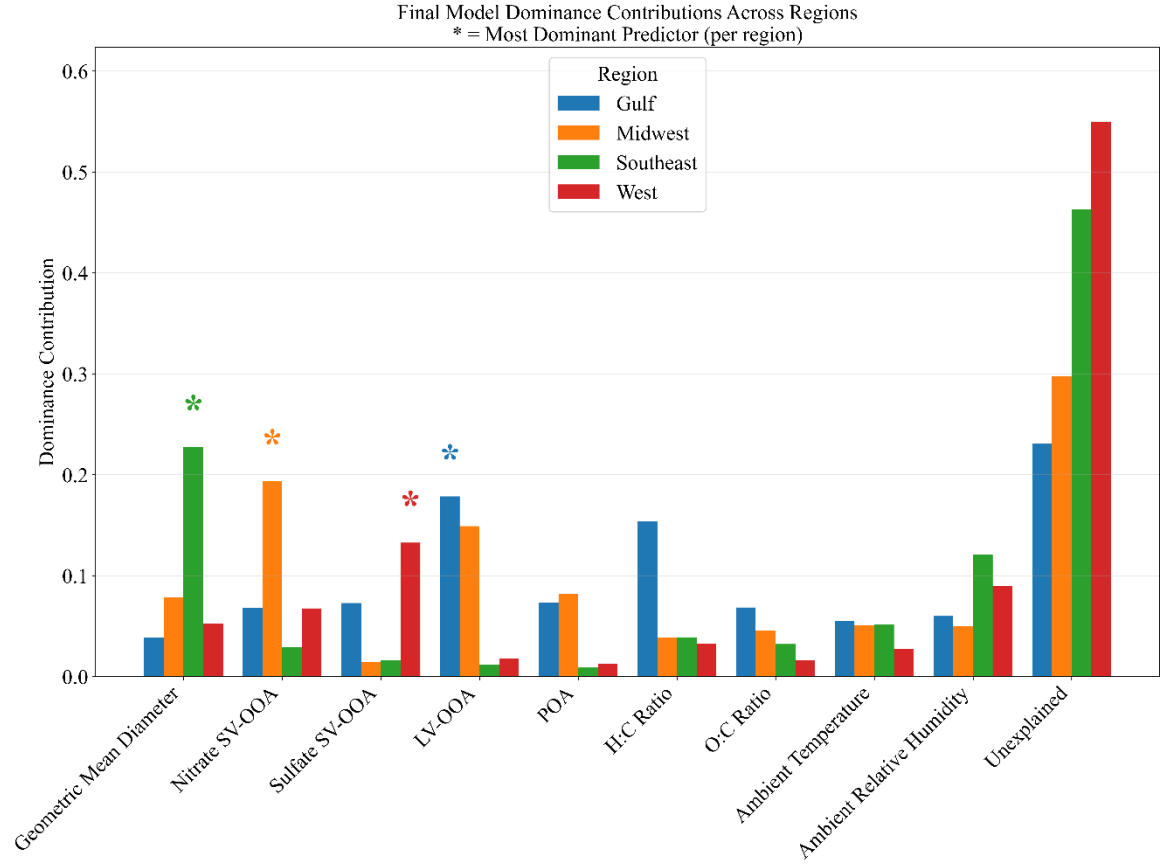


Figure 8. Contribution of each factor to the total variance in the 9-factor model. The star indicates the dominant input per region.

4 Conclusions

In this study, region- and season-specific values of organic hygroscopicity were determined through multiple methods and implemented into a multi-linear regression model. The results in Sections 3.1 and 3.2 generally align with previous studies and the overall estimation of organic hygroscopicity in current modeling, with slight deviations related to mixing states and region and altitude dependencies (Kulkarni et al., 2023; Petters and Kreidenweis, 2007; Pöhlker et al., 2023; Rickards et al., 2013). External mixing with the vertical derivation method in Section 2.3.2 is the favored mixing state and methodology for producing hygroscopicity values closer to expectations from previous literature (Petters and Kreidenweis, 2007; Pöhlker et al., 2023; Rickards et al., 2013). The Western vertical profile was of unique interest, as organic hygroscopicity began increasing above 2000 m. The inability of the AMS to measure refractory components could also play a role in Western US (and other regions) (Canagaratna et al., 2007; Hand et al., 2017). Further research at higher altitudes is needed to further verify if such trend is consistent across regions. Our results show that different approaches to calculating hygroscopicity can lead to Jensen's inequality. By combining PMF results with multivariable linear regression, the region-specific hygroscopicity was derived,

https://doi.org/10.5194/egusphere-2026-6481
Preprint. Discussion started: 5 November 2026
© Author(s) 2026. CC BY 4.0 License.

showing that complexities of microphysical and chemical properties can affect organic hygroscopicity. The defining factors in each region provide an explanation to not only the driving forces in cloud formation, but insight into the formation and reaction pathways of highly important secondary organic aerosols. More studies need to be conducted to elucidate parameters that influence the hygroscopicity of organic species to better understand their impact on current meteorology through rain rates and cloud formation and future climatology through average cloud coverage and radiative forcing, specifically in regions dominated by organic species.

Data availability

All data used in this study are publicly available through the Atmospheric Radiation Measurement (ARM) Data Center (https://www.arm.gov/data). Aerosol chemical composition was measured with the HR-ToF-AMS (Shilling, 2023); particle number size distributions were obtained from the FIMS (Wang, 2016); and cloud condensation nuclei and condensation particle counter data are available in the HI-SCALE campaign datasets (Fast et al., 2016). The HI-SCALE field campaign is described in other studies (Fast et al., 2019).

Author contributions

KM performed the data analysis and wrote the manuscript. YZ supervised the project. JS provided the HR-Tof-AMS data for further analysis. All authors contributed to interpreting the results and editing the manuscript.

Competing interests

The authors declare that they have no competing interests.

Acknowledgements

This research was supported by the United States Department of Energy (DOE) Biological and Environmental Research (BER) Atmospheric System Research (ASR) Grant No. DE-SC0024034. This research was supported by the Atmospheric Radiation Measurement (ARM) User Facility, a U.S. Department of Energy (DOE) Office of Science user facility managed by the Biological and Environmental Research Program. Pacific Northwest National Laboratory (PNNL) authors were supported by U.S. Department of Energy's (DOE) Atmospheric System Research, an Office of Science (SC) Biological and Environmental Research (BER) program. PNNL is operated for the DOE by Battelle Memorial Institute under Contract DE-AC05-76 RL01830. This research was supported by the Office of Biological and Environmental Research (BER) Atmospheric

https://doi.org/10.5194/egusphere-2026-6481
Preprint. Discussion started: 5 November 2026
© Author(s) 2026. CC BY 4.0 License.

Research Program (ASR) in the Department of Energy, Office of Science, and through the U.S. Department of Energy Contract DE-SC0012704 to Brookhaven National Laboratory.

Use of AI tools

During the preparation of this manuscript, the authors used Claude (Anthropic) to assist with formatting the manuscript to the journal template, and refining the Python code used to fine-tune the output style of some figures. The tool was not used to generate scientific content, data, analyses, or their interpretation. The authors reviewed and edited all outputs and take full responsibility for the content of the publication.

References

Ajith, T. C., Windwer, E., Li, C., Fang, Z., Kompalli, S. K., Nursanto, F. R., Olayemi, T. E., Ese, J. I., Sharpe, S. A. L., Fraund, M., Moffet, R. C., Laskin, A., Fry, J. L., and Rudich, Y.: Investigating New Particle Formation and Growth Over an Urban Location in the Eastern Mediterranean, Journal of Geophysical Research: Atmospheres, 129, e2024JD041802, https://doi.org/10.1029/2024JD041802, 2024.

Albrecht, B. A.: Aerosols, cloud microphysics, and fractional cloudiness, Science, 245, 1227–1230, 1989.

Andreae, M. O.: Chapter 10 - Climatic effects of changing atmospheric aerosol levels, in: World Survey of Climatology, edited by: Henderson-Sellers, A., Elsevier, 347–398, https://doi.org/10.1016/S0168-6321(06)80033-7, 1995.

Anwar, K., Alam, K., Liu, Y., Huang, Z., Huang, J., and Liu, Y.: Analysis of aerosol cloud interactions with a consistent signal of meteorology and other influencing parameters, Atmospheric Research, 275, 106241, https://doi.org/10.1016/j.atmosres.2022.106241, 2022.

Arguez, A., Durre, I., Applequist, S., Vose, R. S., Squires, M. F., Yin, X., Heim, R. R., and Owen, T. W.: NOAA's 1981–2010 U.S. Climate Normals: An Overview, Bulletin of the American Meteorological Society, 93, 1687–1697, https://doi.org/10.1175/BAMS-D-11-00197.1, 2012.

Bhattu, D. and Tripathi, S. N.: CCN closure study: Effects of aerosol chemical composition and mixing state, Journal of Geophysical Research: Atmospheres, 120, 766–783, https://doi.org/10.1002/2014JD021978, 2015.

Bibi, R. and Ali, S.: Refining Jensen–Mercer inequality and its applications in probability and statistics, Journal of Inequalities and Applications, 2025, 86, 10.1186/s13660-025-03314-6, 2025.

Broekhuizen, K., Chang, R. Y. W., Leaitch, W. R., Li, S. M., and Abbatt, J. P. D.: Closure between measured and modeled cloud condensation nuclei (CCN) using size-resolved aerosol compositions in downtown Toronto, Atmos. Chem. Phys., 6, 2513–2524, 10.5194/acp-6-2513-2006, 2006.

Brown, S. G., Eberly, S., Paatero, P., and Norris, G. A.: Methods for estimating uncertainty in PMF solutions: Examples with ambient air and water quality data and guidance on reporting PMF results, Science of The Total Environment, 518-519, 626–635, https://doi.org/10.1016/j.scitotenv.2015.01.022, 2015.

Canagaratna, M. R., Jayne, J. T., Jimenez, J. L., Allan, J. D., Alfarra, M. R., Zhang, Q., Onasch, T. B., Drewnick, F., Coe, H., Middlebrook, A., Delia, A., Williams, L. R., Trimborn, A. M., Northway, M. J., DeCarlo, P. F., Kolb, C. E., Davidovits, P., and Worsnop, D. R.: Chemical and microphysical characterization of ambient aerosols with the Aerodyne aerosol mass spectrometer, Mass Spectrometry Reviews, 26, 185–222, 10.1002/mas.20115, 2007.

Cerully, K. M., Bougiatioti, A., Hite Jr, J. R., Guo, H., Xu, L., Ng, N. L., Weber, R., and Nenes, A.: On the link between hygroscopicity, volatility, and oxidation state of ambient and water-soluble aerosols in the southeastern United States, Atmos. Chem. Phys., 15, 8679–8694, 10.5194/acp-15-8679-2015, 2015.

Chang, R. Y. W., Slowik, J. G., Shantz, N. C., Vlasenko, A., Liggio, J., Sjostedt, S. J., Leaitch, W. R., and Abbatt, J. P. D.: The hygroscopicity parameter (κ) of ambient organic aerosol at a field site subject to biogenic and anthropogenic influences: relationship to degree of aerosol oxidation, Atmos. Chem. Phys., 10, 5047–5064, 10.5194/acp-10-5047-2010, 2010.

DeCarlo, P. F., Kimmel, J. R., Trimborn, A., Northway, M. J., Jayne, J. T., Aiken, A. C., Gonin, M., Fuhrer, K., Horvath, T., Docherty, K. S., Worsnop, D. R., and Jimenez, J. L.: Field-Deployable, High-Resolution, Time-of-Flight Aerosol Mass Spectrometer, Analytical Chemistry, 78, 8281–8289, 10.1021/ac061249n, 2006.

https://doi.org/10.5194/egusphere-2026-6481
Preprint. Discussion started: 5 November 2026
© Author(s) 2026. CC BY 4.0 License.

Dinar, E., Anttila, T., and Rudich, Y.: CCN Activity and Hygroscopic Growth of Organic Aerosols Following Reactive Uptake of Ammonia, Environmental Science & Technology, 42, 793–799, 10.1021/es071874p, 2008.
Draxler, R. and Rolph, G.: HYSPLIT (HYbrid Single-Particle Lagrangian Integrated Trajectory) model access via NOAA ARL READY website (http://ready. arl. noaa. gov/HYSPLIT. php). NOAA Air Resources Laboratory, Silver Spring, MD, 25, 2010.
Drosatou, A. D., Skyllakou, K., Theodoritsi, G. N., and Pandis, S. N.: Positive matrix factorization of organic aerosol: insights from a chemical transport model, Atmos. Chem. Phys., 19, 973–986, 10.5194/acp-19-973-2019, 2019.
Duplissy, J., Gysel, M., Alfarra, M. R., Dommen, J., Metzger, A., Prevot, A. S. H., Weingartner, E., Laaksonen, A., Raatikainen, T., Good, N., Turner, S. F., McFiggans, G., and Baltensperger, U.: Cloud forming potential of secondary organic aerosol under near atmospheric conditions, Geophysical Research Letters, 35, https://doi.org/10.1029/2007GL031075, 2008.
Duplissy, J., DeCarlo, P. F., Dommen, J., Alfarra, M. R., Metzger, A., Barmpadimos, I., Prevot, A. S. H., Weingartner, E., Tritscher, T., Gysel, M., Aiken, A. C., Jimenez, J. L., Canagaratna, M. R., Worsnop, D. R., Collins, D. R., Tomlinson, J., and Baltensperger, U.: Relating hygroscopicity and composition of organic aerosol particulate matter, Atmos. Chem. Phys., 11, 1155–1165, 10.5194/acp-11-1155-2011, 2011.
Falah, S., Mhawish, A., Omar, A. H., Sorek-Hamer, M., Lyapustin, A. I., Banerjee, T., Kizel, F., and Broday, D. M.: Intercomparison of Aerosol Types Reported as Part of Aerosol Product Retrieval over Diverse Geographic Regions, Remote Sensing, 14, 3667, 2022.
Fan, J., Wang, Y., Rosenfeld, D., and Liu, X.: Review of Aerosol–Cloud Interactions: Mechanisms, Significance, and Challenges, Journal of the Atmospheric Sciences, 73, 4221–4252, https://doi.org/10.1175/JAS-D-16-0037.1, 2016.
Fast, J., Mei, F., Hubbe, J., Kalukin, A., Long, C., Matthews, A., Pekour, M., Schobesberger, S., Shilling, J., Springston, S., Tomlinson, J., Wang, J., and Zelenyuk-Imre, A.: Campaign Datasets for the Holistic Interactions of Shallow Clouds, Aerosols, and Land-Ecosystems (HI-SCALE), Atmospheric Radiation Measurement (ARM) User Facility [dataset], 10.5439/1345492, 2016.
Fast, J. D., Berg, L. K., Alexander, L., Bell, D., D'Ambro, E., Hubbe, J., Kuang, C., Liu, J., Long, C., Matthews, A., Mei, F., Newsom, R., Pekour, M., Pinterich, T., Schmid, B., Schobesberger, S., Shilling, J., Smith, J. N., Springston, S., Suski, K., Thornton, J. A., Tomlinson, J., Wang, J., Xiao, H., and Zelenyuk, A.: Overview of the HI-SCALE Field Campaign: A New Perspective on Shallow Convective Clouds, Bulletin of the American Meteorological Society, 100, 821–840, https://doi.org/10.1175/BAMS-D-18-0030.1, 2019.
Gunthe, S. S., King, S. M., Rose, D., Chen, Q., Roldin, P., Farmer, D. K., Jimenez, J. L., Artaxo, P., Andreae, M. O., Martin, S. T., and Pöschl, U.: Cloud condensation nuclei in pristine tropical rainforest air of Amazonia: size-resolved measurements and modeling of atmospheric aerosol composition and CCN activity, Atmospheric Chemistry and Physics, 9, 7551–7575, 10.5194/acp-9-7551-2009, 2009.
Gysel, M., Crosier, J., Topping, D. O., Whitehead, J. D., Bower, K. N., Cubison, M. J., Williams, P. I., Flynn, M. J., McFiggans, G. B., and Coe, H.: Closure study between chemical composition and hygroscopic growth of aerosol particles during TORCH2, Atmos. Chem. Phys., 7, 6131–6144, 10.5194/acp-7-6131-2007, 2007.
Han, S., Hong, J., Luo, Q., Xu, H., Tan, H., Wang, Q., Tao, J., Zhou, Y., Peng, L., He, Y., Shi, J., Ma, N., Cheng, Y., and Su, H.: Hygroscopicity of organic compounds as a function of organic functionality, water solubility, molecular weight, and oxidation level, Atmos. Chem. Phys., 22, 3985–4004, 10.5194/acp-22-3985-2022, 2022.
Hand, J. L., Gill, T. E., and Schichtel, B. A.: Spatial and seasonal variability in fine mineral dust and coarse aerosol mass at remote sites across the United States, Journal of Geophysical Research: Atmospheres, 122, 3080–3097, 10.1002/2016jd026290, 2017.
Hobbs, P. V.: Chapter 2 Aerosol-Cloud Interactions, in: International Geophysics, edited by: Hobbs, P. V., Academic Press, 33–73, https://doi.org/10.1016/S0074-6142(08)60211-9, 1993.
Hu, D., Qiao, L., Chen, J., Ye, X., Yang, X., Cheng, T., and Fang, W.: Hygroscopicity of Inorganic Aerosols: Size and Relative Humidity Effects on the Growth Factor, Aerosol and Air Quality Research, 10, 255–264, 10.4209/aaqr.2009.12.0076, 2010.
Intergovernmental Panel on Climate, C.: Climate Change 2023: Synthesis Report
Climate Change 2023: Synthesis Report. Contribution of Working Groups I, II and III to the Sixth Assessment Report of the Intergovernmental Panel on Climate Change, IPCC, Geneva, Switzerland, 2023.

https://doi.org/10.5194/egusphere-2026-6481
Preprint. Discussion started: 5 November 2026
© Author(s) 2026. CC BY 4.0 License.

Jayachandran, V., Nair, V. S., and Babu, S. S.: CCN characteristics over a tropical coastal station during south-west monsoon: observations and closure studies, Atmospheric Environment, 164, 299–308, https://doi.org/10.1016/j.atmosenv.2017.06.012, 2017.

Jayne, J. T., Leard, D. C., Zhang, X., Davidovits, P., Smith, K. A., Kolb, C. E., and Worsnop, D. R.: Development of an Aerosol Mass Spectrometer for Size and Composition Analysis of Submicron Particles, Aerosol Science and Technology, 33, 49–70, 10.1080/027868200410840, 2000.

Kroll, J. H., Lim, C. Y., Kessler, S. H., and Wilson, K. R.: Heterogeneous Oxidation of Atmospheric Organic Aerosol: Kinetics of Changes to the Amount and Oxidation State of Particle-Phase Organic Carbon, The Journal of Physical Chemistry A, 119, 10767–10783, 10.1021/acs.jpca.5b06946, 2015.

Kuang, Y., He, Y., Xu, W., Zhao, P., Cheng, Y., Zhao, G., Tao, J., Ma, N., Su, H., Zhang, Y., Sun, J., Cheng, P., Yang, W., Zhang, S., Wu, C., Sun, Y., and Zhao, C.: Distinct diurnal variation in organic aerosol hygroscopicity and its relationship with oxygenated organic aerosol, Atmos. Chem. Phys., 20, 865–880, 10.5194/acp-20-865-2020, 2020.

Kulkarni, G., Mei, F., Shilling, J. E., Wang, J., Reveggino, R. P., Flynn, C., Zelenyuk, A., and Fast, J.: Cloud Condensation Nuclei Closure Study Using Airborne Measurements Over the Southern Great Plains, Journal of Geophysical Research: Atmospheres, 128, e2022JD037964, https://doi.org/10.1029/2022JD037964, 2023.

Lambe, A. T., Onasch, T. B., Massoli, P., Croasdale, D. R., Wright, J. P., Ahern, A. T., Williams, L. R., Worsnop, D. R., Brune, W. H., and Davidovits, P.: Laboratory studies of the chemical composition and cloud condensation nuclei (CCN) activity of secondary organic aerosol (SOA) and oxidized primary organic aerosol (OPOA), Atmos. Chem. Phys., 11, 8913–8928, 10.5194/acp-11-8913-2011, 2011.

Lance, S., Nenes, A., Medina, J., and Smith, J. N.: Mapping the Operation of the DMT Continuous Flow CCN Counter, Aerosol Science and Technology, 40, 242–254, 10.1080/02786820500543290, 2006.

Li, W., Sun, J., Xu, L., Shi, Z., Riemer, N., Sun, Y., Fu, P., Zhang, J., Lin, Y., Wang, X., Shao, L., Chen, J., Zhang, X., Wang, Z., and Wang, W.: A conceptual framework for mixing structures in individual aerosol particles, Journal of Geophysical Research: Atmospheres, 121, 13,784–713,798, https://doi.org/10.1002/2016JD025252, 2016.

Liu, P. S. K., Deng, R., Smith, K. A., Williams, L. R., Jayne, J. T., Canagaratna, M. R., Moore, K., Onasch, T. B., Worsnop, D. R., and Deshler, T.: Transmission Efficiency of an Aerodynamic Focusing Lens System: Comparison of Model Calculations and Laboratory Measurements for the Aerodyne Aerosol Mass Spectrometer, Aerosol Science and Technology, 41, 721–733, 10.1080/02786820701422278, 2007.

Loveland, T. R., Merchant, J. W., Brown, J. F., Ohlen, D. O., Reed, B. C., Olson, P., and Hutchinson, J.: Seasonal Land-Cover Regions of the United States, Annals of the Association of American Geographers, 85, 339–355, https://doi.org/10.1111/j.1467-8306.1995.tb01797.x-i1, 1995.

Massoli, P., Lambe, A. T., Ahern, A. T., Williams, L. R., Ehn, M., Mikkilä, J., Canagaratna, M. R., Brune, W. H., Onasch, T. B., Jayne, J. T., Petäjä, T., Kulmala, M., Laaksonen, A., Kolb, C. E., Davidovits, P., and Worsnop, D. R.: Relationship between aerosol oxidation level and hygroscopic properties of laboratory generated secondary organic aerosol (SOA) particles, Geophysical Research Letters, 37, https://doi.org/10.1029/2010GL045258, 2010.

Meng, J. W., Yeung, M. C., Li, Y. J., Lee, B. Y. L., and Chan, C. K.: Size-resolved cloud condensation nuclei (CCN) activity and closure analysis at the HKUST Supersite in Hong Kong, Atmos. Chem. Phys., 14, 10267–10282, 10.5194/acp-14-10267-2014, 2014.

Miao, Q., Zhang, Z., Li, Y., Qin, X., Xu, B., Yuan, Y., and Gao, Z.: Measurement of cloud condensation nuclei (CCN) and CCN closure at Mt. Huang based on hygroscopic growth factors and aerosol number-size distribution, Atmospheric Environment, 113, 127–134, https://doi.org/10.1016/j.atmosenv.2015.05.006, 2015.

Mohr, C., DeCarlo, P. F., Heringa, M. F., Chirico, R., Slowik, J. G., Richter, R., Reche, C., Alastuey, A., Querol, X., Seco, R., Peñuelas, J., Jiménez, J. L., Crippa, M., Zimmermann, R., Baltensperger, U., and Prévôt, A. S. H.: Identification and quantification of organic aerosol from cooking and other sources in Barcelona using aerosol mass spectrometer data, Atmos. Chem. Phys., 12, 1649–1665, 10.5194/acp-12-1649-2012, 2012.

Mülmenstädt, J. and Feingold, G.: The Radiative Forcing of Aerosol–Cloud Interactions in Liquid Clouds: Wrestling and Embracing Uncertainty, Current Climate Change Reports, 4, 23–40, 10.1007/s40641-018-0089-y, 2018.

Nimon, K. F. and Oswald, F. L.: Understanding the Results of Multiple Linear Regression:Beyond Standardized Regression Coefficients, Organizational Research Methods, 16, 650–674, 10.1177/1094428113493929, 2013.

https://doi.org/10.5194/egusphere-2026-6481
Preprint. Discussion started: 5 November 2026
© Author(s) 2026. CC BY 4.0 License.

Nursanto, F. R., Meinen, R., Holzinger, R., Krol, M. C., Liu, X., Dusek, U., Henzing, B., and Fry, J. L.: What chemical species are responsible for new particle formation and growth in the Netherlands? A hybrid positive matrix factorization (PMF) analysis using aerosol composition (ACSM) and size (SMPS), Atmos. Chem. Phys., 23, 10015–10034, 10.5194/acp-23-10015-2023, 2023.

Ovadnevaite, J., Ceburnis, D., Martucci, G., Bialek, J., Monahan, C., Rinaldi, M., Facchini, M. C., Berresheim, H., Worsnop, D. R., and O'Dowd, C.: Primary marine organic aerosol: A dichotomy of low hygroscopicity and high CCN activity, Geophysical Research Letters, 38, https://doi.org/10.1029/2011GL048869, 2011.

Park, M., Yum, S. S., Kim, N., Anderson, B. E., Beyersdorf, A., and Thornhill, K. L.: On the submicron aerosol distributions and CCN activity in and around the Korean Peninsula measured onboard the NASA DC-8 research aircraft during the KORUS-AQ field campaign, Atmospheric Research, 243, 105004, 2020.

Petters, M. D. and Kreidenweis, S. M.: A single parameter representation of hygroscopic growth and cloud condensation nucleus activity, Atmos. Chem. Phys., 7, 1961–1971, 10.5194/acp-7-1961-2007, 2007.

Pöhlker, M. L., Pöhlker, C., Quaas, J., Mülmenstädt, J., Pozzer, A., Andreae, M. O., Artaxo, P., Block, K., Coe, H., Ervens, B., Gallimore, P., Gaston, C. J., Gunthe, S. S., Henning, S., Herrmann, H., Krüger, O. O., McFiggans, G., Poulain, L., Raj, S. S., Reyes-Villegas, E., Royer, H. M., Walter, D., Wang, Y., and Pöschl, U.: Global organic and inorganic aerosol hygroscopicity and its effect on radiative forcing, Nature Communications, 14, 6139, 10.1038/s41467-023-41695-8, 2023.

Pratt, J. W.: Concavity of the Log Likelihood, Journal of the American Statistical Association, 76, 103–106, 10.2307/2287052, 1981.

Ren, J., Zhang, F., Wang, Y., Collins, D., Fan, X., Jin, X., Xu, W., Sun, Y., Cribb, M., and Li, Z.: Using different assumptions of aerosol mixing state and chemical composition to predict CCN concentrations based on field measurements in urban Beijing, Atmos. Chem. Phys., 18, 6907–6921, 10.5194/acp-18-6907-2018, 2018.

Rickards, A. M. J., Miles, R. E. H., Davies, J. F., Marshall, F. H., and Reid, J. P.: Measurements of the Sensitivity of Aerosol Hygroscopicity and the κ Parameter to the O/C Ratio, The Journal of Physical Chemistry A, 117, 14120–14131, 10.1021/jp407991n, 2013.

Riemer, N., Ault, A. P., West, M., Craig, R. L., and Curtis, J. H.: Aerosol Mixing State: Measurements, Modeling, and Impacts, Reviews of Geophysics, 57, 187–249, https://doi.org/10.1029/2018RG000615, 2019.

Rissman, T., Nenes, A., and Seinfeld, J.: Chemical amplification (or dampening) of the Twomey effect: Conditions derived from droplet activation theory, Journal of the atmospheric sciences, 61, 919–930, 2004.

Roberts, G. C. and Nenes, A.: A Continuous-Flow Streamwise Thermal-Gradient CCN Chamber for Atmospheric Measurements, Aerosol Science and Technology, 39, 206–221, 10.1080/027868290913988, 2005.

Rosenfeld, D., Sherwood, S., Wood, R., and Donner, L.: Climate Effects of Aerosol-Cloud Interactions, Science, 343, 379–380, doi:10.1126/science.1247490, 2014.

Seinfeld, J. H. and Pandis, S. N.: Atmospheric chemistry and physics: from air pollution to climate change, John Wiley & Sons2016.

Shilling, J. E.: HI-SCALE IOP1 and IOP2 G-1 HR-ToF-AMS, Atmospheric Radiation Measurement (ARM) User Facility [dataset], 10.5439/1908795, 2023.

Srivastava, M., Tripathi, S. N., Dwivedi, A. K., Dalai, R., Bhattu, D., Bharti, P. K., Jaidevi, J., and Gupta, T.: CCN closure results from Indian Continental Tropical Convergence Zone (CTCZ) aircraft experiment, Atmospheric Research, 132-133, 322–331, https://doi.org/10.1016/j.atmosres.2013.05.025, 2013.

T. C., A., Kompalli, S. K., and Babu, S. S.: Role of Aerosol Physicochemical Properties on Aerosol Hygroscopicity and Cloud Condensation Nuclei Activity in a Tropical Coastal Atmosphere, ACS Earth and Space Chemistry, 6, 1527–1542, 10.1021/acsearthspacechem.2c00044, 2022.

Twomey, S.: The influence of pollution on the shortwave albedo of clouds, Journal of Atmospheric Sciences, 34, 1149–1152, 1977.

Uyanık, G. K. and Güler, N.: A Study on Multiple Linear Regression Analysis, Procedia - Social and Behavioral Sciences, 106, 234–240, https://doi.org/10.1016/j.sbspro.2013.12.027, 2013.

VanReken, T. M., Rissman, T. A., Roberts, G. C., Varutbangkul, V., Jonsson, H. H., Flagan, R. C., and Seinfeld, J. H.: Toward aerosol/cloud condensation nuclei (CCN) closure during CRYSTAL-FACE, Journal of Geophysical Research: Atmospheres, 108, https://doi.org/10.1029/2003JD003582, 2003.

https://doi.org/10.5194/egusphere-2026-6481
Preprint. Discussion started: 5 November 2026
© Author(s) 2026. CC BY 4.0 License.



Wang, J.: HI-SCALE G-1 Fast Integrated Mobility Spectrometer (FIMS): Particle Number Size Distributions, 10-400 nm, Atmospheric Radiation Measurement (ARM) User Facility [dataset], 10.5439/1867567, 2016.

Wang, J., Pikridas, M., Spielman, S. R., and Pinterich, T.: A Fast Integrated Mobility Spectrometer for Rapid Measurement of Sub-Micrometer Aerosol Size Distribution, Part I: Design and Model Evaluation, Journal of Aerosol Science, 108, 44–55, 10.1016/j.jaerosci.2017.02.012, 2017.

Wang, Y., Pinterich, T., and Wang, J.: Rapid measurement of sub-micrometer aerosol size distribution using a fast integrated mobility spectrometer, Journal of Aerosol Science, 121, 12–20, https://doi.org/10.1016/j.jaerosci.2018.03.006, 2018.

Xiao, L. and Lu, G.: A new refinement of Jensen's inequality with applications in information theory, Open Mathematics, 18, 1748–1759, doi:10.1515/math-2020-0123, 2020.